JMEPEG (2013) 22:1378–1385
DOI: 10.1007/s11665-012-0434-6

1059-9495/$19.00

Kinetic Parameters of Secondary Carbide Precipitation in High-Cr White Iron Alloyed by Mn-Ni-Mo-V Complex

V.G. Efremenko, Yu.G. Chabak, and M.N. Brykov

(Submitted September 14, 2012; in revised form October 26, 2012; published online November 29, 2012)

This study presents kinetics of precipitation of secondary carbides in 14.55%Cr-Mn-Ni-Mo-V white cast iron during the destabilization heat treatment. The as-cast iron was heat treated at temperatures in the range of 800-1100 °C with soaking up to 6 h. Investigation was carried out by optical and electron microscopy, dilatometric analysis, Ms temperature measurement, and bulk hardness evaluation. TTT-curve of precipitation process of secondary carbides (M_7C_3, $M_{23}C_6$, M_3C_2) has been constructed in this study. It was determined that the precipitation occurs at the maximum rate at 950 °C where the process is started after 10 s and completed within 160 min further. The precipitation leads to significant increase of Ms temperature and bulk hardness; large soaking times at destabilization temperatures cause coarsening of secondary carbides and decrease in particles number, followed by decrease in hardness. The results obtained are discussed in terms of solubility of carbon in the austenite and diffusion activation of Cr atoms. The precipitation was found to consist of two stages with activation energies of 196.5 kJ/g-mole at the first stage and 47.1 kJ/g-mole at the second stage.

Keywords cast irons, heat treating, optical microscopy

1. Introduction

White cast high-Cr cast irons are widely used as materials for tribological applications because of their excellent abrasive and corrosive-abrasive wear resistance properties (Ref 1, 2). The structure of white hypoeutectic cast irons consists of dendrites and eutectic carbides in interdendritic regions. High-Cr irons, alloyed by increased amounts of Mn, Ni, Mo, and Cu, are known to have fully austenitic structure of dendrites. The primary austenite which is formed during the crystallization has high stability to $\gamma \rightarrow \alpha$ (perlite or martensite) transformation on being cooled to ambient temperature. At the same time, the primary austenite is considered to be thermodynamically unstable because of its supersaturation by carbon and alloying elements. Thereby, austenite is prone to carbides precipitation that may change its stability to phase transformation.

As a rule, high-Cr white iron castings are subjected to destabilizing heat treatment with the purpose of increasing the wear performance of castings. During this treatment, primary austenite decomposes with the subsequent precipitation of secondary carbides (Ref 3–8). Because of γ-phase depletion of C and Cr followed by precipitation, the martensite transformation start temperature (Ms) rises affecting the appearance of a significant amount of martensite in matrix after heat treatment. Thus, destabilization leads to increase in the bulk hardness and the abrasive wear resistance of cast irons(Ref 3). Destabilizing heat treatment is usually via heating at temperature range of 800-1100 °C with soaking period of several hours. The optimal destabilization regime can be found on the base of precipitation kinetics data. The kinetics of precipitation of secondary carbides in high-Cr cast irons was studied by Maratray (Ref 9), Bedolla-Jacuinde (Ref 3), and Weingmoon et al. (Ref 7). The evaluation of dynamic parameters of precipitation of secondary carbides in high-Cr superalloy was made by Lothongkum et al. (Ref 10). Despite these efforts, there is a shortage of systematic research data on precipitation kinetics in white cast irons. This especially concerns high-Cr cast iron alloyed by addition of elements which substantially increase austenite stability to phase transformation.

The objective of the current study is to study the kinetics features of precipitation of secondary carbides upon destabilization in high-Cr white iron alloyed by complex Mn-Ni-Mo-V.

2. Experimental Procedure

High-Cr cast iron was prepared by melting in induction furnace. Molten iron was poured into CO_2-treated sand mold to form bars with cross section: 25 × 25 mm and total length, 250 mm. The chemical composition of the alloy is shown in Table 1.

The cast bars were cut by abrasive disk to obtain the 10 × 10 × 2 mm samples. Water-based emulsion was used for cooling to avoid overheating of the samples.

As-cast iron was destabilized in electric muffle furnace at 800, 850, 900, 950, 1000, 1050, and 1100 °C up to 360 min. No controlled atmosphere was used. The temperature of the sample during destabilization was monitored by a computer

V.G. Efremenko and **Yu.G. Chabak**, Department of Metal Science and Heat Treatment of Metals, Pryazovskyi State Technical University, ul. Universitetskaya 7, Mariupol 87500, Ukraine; and **M.N. Brykov**, Department of Welding, Zaporozh'e National Technical University, ul. Zhukovskogo 64, Zaporozh'e 69063, Ukraine. Contact e-mails: vgefremenko@rambler.ru, vgefremenko@mail.ru, julia.chabak@yandex.ua, and m@brykov.com.

Table 1 Chemical composition of cast iron

Elements, mass. %							
C	Cr	Si	Mn	Ni	Mo	V	Ti
2.70	14.55	0.55	2.20	0.93	0.39	0.38	0.11

using a chromel-alumel thermocouple welded to the sample. After soaking, the samples were cooled in the air, and cooling curves were recorded.

The Ms temperature was found by inflection point on the cooling curves attributed to release of phase transformation heat.

After destabilization, the bulk hardness tests were fulfilled by Rockwell method, C-scale. The samples were ground and polished according to a standard procedure, and then they were etched by solution of 4 mL HNO_3 in 100 mL of ethanol. Microstructure study was undertaken by optical metallographic microscope (Zeiss Axiovert 40 MAT) and SEM (Zeiss Ultra 55).

The number of precipitated carbides particles in a square micron within dendrite regions was calculated using point counting measurements on SEM micrographs.

The critical point Ac_1 of cast iron was determined by analyzing with optical mirror dilatometer. Previously, the samples of 20-mm length and 2-mm diameter were destabilized at 950 °C for 2 h to obtain martensite with the purpose of detecting the volumetric effect of $\alpha \rightarrow \gamma$ phase transformation. The dilatometric heating curves were recorded by light beam deflection fixed on the screen, which was located at a distance of 600 mm from the mirror.

The data of phases presented in alloy were obtained by XRD investigation using Rigaku Ultra IV Pro diffractometer in Cu-K*a* radiation in the angle range of 30-150 °C.

3. Results and Discussion

Dilatometric heating curve of cast iron studied is shown in Fig. 1. As seen on the curve, there is a significant volume decrease resulted by $\alpha \rightarrow \gamma$ transformation at 760-820 °C, which can be attributed to critical temperature interval (Ac_1 point) of alloy. Taking this into account, the minimal destabilization temperature (800 °C) was chosen close to upper limit of the critical interval to avoid the superposition of $\alpha \rightarrow \gamma$ transformation and the precipitation of secondary carbides which makes microstructure identification too difficult.

3.1 Microstructure Observation

The metallographic study showed that in as-cast condition, cast iron consists of austenite dendrites and eutectic carbides. The samples had a slight magnetic property indicating the presence of α-phase which lies in a narrow band near the eutectic carbides.

The destabilization significantly affects the cast iron microstructure, causing the precipitation of secondary carbides and martensite transformation. At any destabilization temperature, the formation of secondary carbides starts at dendrites areas directly adjacent to the eutectic carbides and then progresses toward the center of dendrites. At 800-950 °C after short

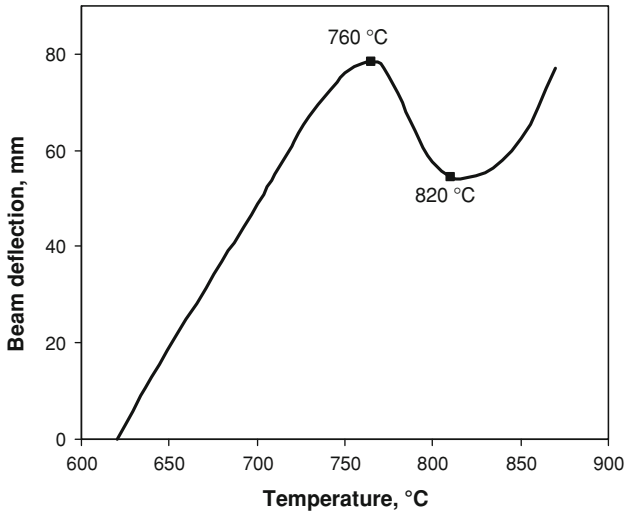

Fig. 1 Dilatometric heating curve of alloy

soaking (5-10 min), the dark contour appears around eutectic colonies. That contour is formed by very fine carbide particles, which could be resolved only in SEM (Fig. 2a). During further soaking, the secondary carbides precipitate throughout the dendrites' region. At destabilization temperature range of 800-850 °C, the secondary carbides maintain their small size; after 4-6 h of soaking, the dendrites matrix became uniformly dark because of enhanced etching due to the presence of large number of disperse carbide particles (Fig. 2b). The number of precipitated particles per square micron changes very slightly during soaking within the time range of 80 min-6 h (Fig. 3).

At 900-950 °C, the precipitation also proceeds via "dark contour formation" stage. However, after about 20-min soaking, the separate secondary carbides can be distinguished by optical microscope that indicates their enlarged size (Fig. 4a). The particles have mostly cubic form, but there are some with elongated plate-like shape (Fig. 4b). It is necessary to highlight that after soaking at 900-950 °C for 80-100 min, the secondary carbides lying close to eutectics are obviously smaller than those in the region inside dendrites. This observation agrees with the results reported by Wiengmoon et al. (Ref 7). With further holding at 950 °C the coarsening of carbides (Ostwald ripening process) is clearly seen. After 6 h of destabilization, the fine secondary carbides could not be found in structure; instead, just coarse carbides could be observed as uniformly distributed inside dendrites (Fig. 4c). The number of total particle distribution significantly decreased from 7 to 8 particles per μm^2 during the 40-80 min soaking time, to 1.1 particles during the 6-h saoking (Fig. 3). A similar coarsening process in destabilized high-Cr cast irons was previously described in Ref 3, 11. When carbides are coarsened, the martensite plates can be seen because of austenite grain enlargement.

At higher destabilization temperatures (1000-1050 °C), the decomposition of γ-phase quickly passes "dark contour formation" stage, and after 2-5-min soaking time, large secondary carbides can be observed close to eutectic carbides (Fig. 5a). As follows from Fig. 3, the precipitated particles number reached maximum value after short soaking: 3.6 and 0.9 particles per μm^2 at 1000 and 1050 °C, respectively. During further soaking, precipitation process is accompanied with the coarsening of secondary carbides, that leads to particles number

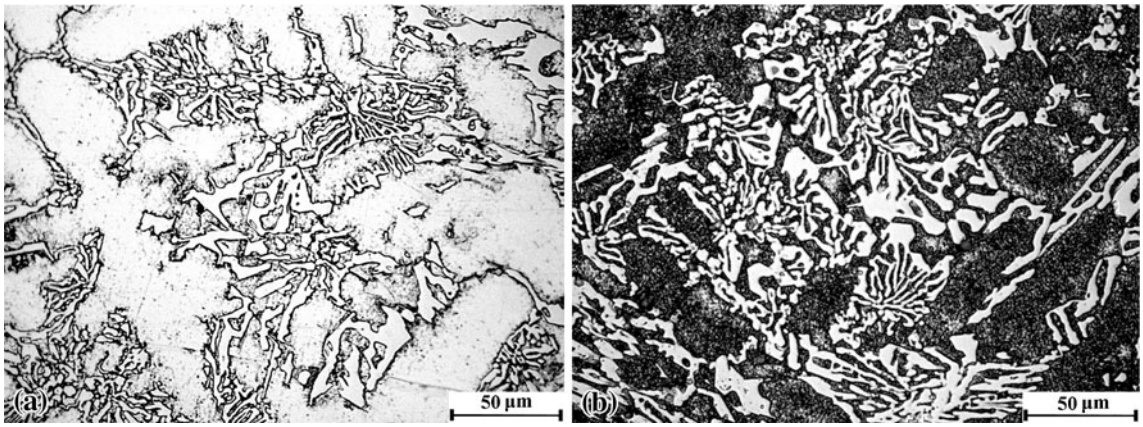

Fig. 2 Microstructure of cast alloy after destabilization at 800 °C for 10 min (a) and 6 h (b)

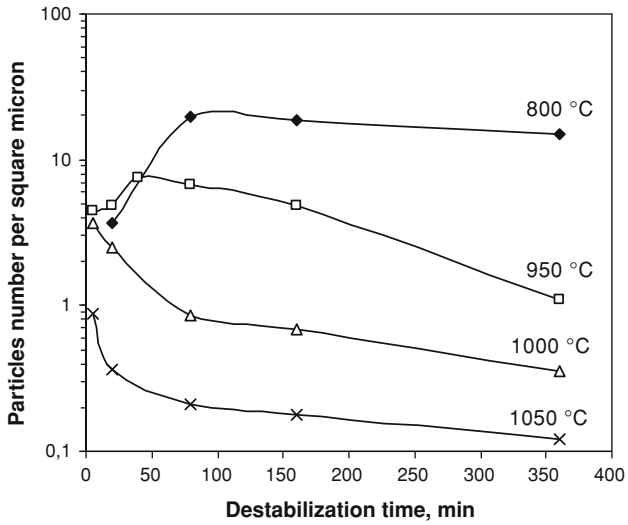

Fig. 3 Number of precipitated carbides particles in a square micron as a function of destabilization time at different temperatures

decrease. Even reverse dissolution of secondary carbides in the areas near eutectic carbides was indicated at 1050 °C (Fig. 5b).

The precipitation process in the current study was found to progress from dendrites periphery to its center. This result corresponds to data obtained by Kuwano (Ref 11), Laird and Powell (Ref 12), but contradicts the study by Bedolla-Jacuinde (Ref 3) where precipitation of secondary carbides in high-Cr cast iron was observed homogeneously in dendrites. In Ref 10, the phenomenon of precipitation start near eutectic carbides is explained by chromium and carbon micro-segregation at dendrites periphery. Such segregation really was found by Powell and Laird II (Ref 13) who revealed the chromium content decreasing within 2 µm wide zone just close to eutectic carbide. This fact does not give a clear explanation of the results obtained. On the one hand, chromium slows down the diffusion of carbon atoms so its deficiency should accelerate precipitation of secondary carbides. On the other hand, the precipitation process requires Cr atoms because secondary carbides of M_7C_3 type contain 45-50% Cr (Ref 14). Moreover, it is known that chromium reduces the solubility of carbon in γ-phase. Thus, the chromium depletion may increase the austenite stability to carbides precipitation. In view of the above, another explanation could be offered.

It is known that new phases appear mainly heterogeneously in places where it is thermodynamically more favorable, mostly on clusters of crystal defects, sub-grain boundaries, other defects sites where, the atoms' diffusion is furthermore accelerated. In the current study, secondary carbides were found to nucleate along slip bands. The austenite regions adjacent to the eutectic carbides presumably contain higher amount of lattice defects as a result of plastic deformation generated by difference in thermal expansion coefficients of matrix and eutectic carbides. The concentration of defects inside the dendrites areas is reduced as far as during solidification and cooling to ambient temperature in these places no phase transformation induced deformation took place. Based on these assumptions, the small size of secondary carbides close to eutectic carbides could be explained by the presence of a large number of sites (such as defects clusters) where more carbides of critical size should nucleate because of reduced activation energy.

3.2 Phase Composition Determination

According to XRD pattern (Fig. 6a) as-cast alloy structure consists of austenite, α-phase (martensite or ferrite) and eutectic chromium rich carbides type M_7C_3. The α-phase amount in matrix as measured by XRD is about 15%.

After destabilization at 950 °C for 4 h the alloy phase composition changed. Comparing Fig. 6a and (b) one can say that there are more peaks of carbides type M_7C_3 on XRD pattern of destabilized sample. Also, the traces of other carbides types—$M_{23}C_6$ and M_3C_2—were distinguished on the pattern. The alloy matrix consists of austenite and α-phases, while the amount of α-phase is higher than in as-cast state—38 %. Based on the microstructural change, it should be concluded that α-phase in destabilized sample is martensite.

The analysis of XRD patterns show that the secondary carbides precipitated during destabilization are mostly M_7C_3, which can be seen from XRD traces. Apart of M_7C_3, two other carbides ($M_{23}C_6$ and M_3C_2) are precipitated in the alloy, although their amount is much less than M_7C_3 one.

3.3 Ms Temperature Measurement

Thus, it was found that the destabilization causes an intensive precipitation of secondary carbides, which leads to depletion of γ-phase with carbon and carbide-forming elements (Cr, Mn, Mo, and V) influencing on Ms temperature. The Ms

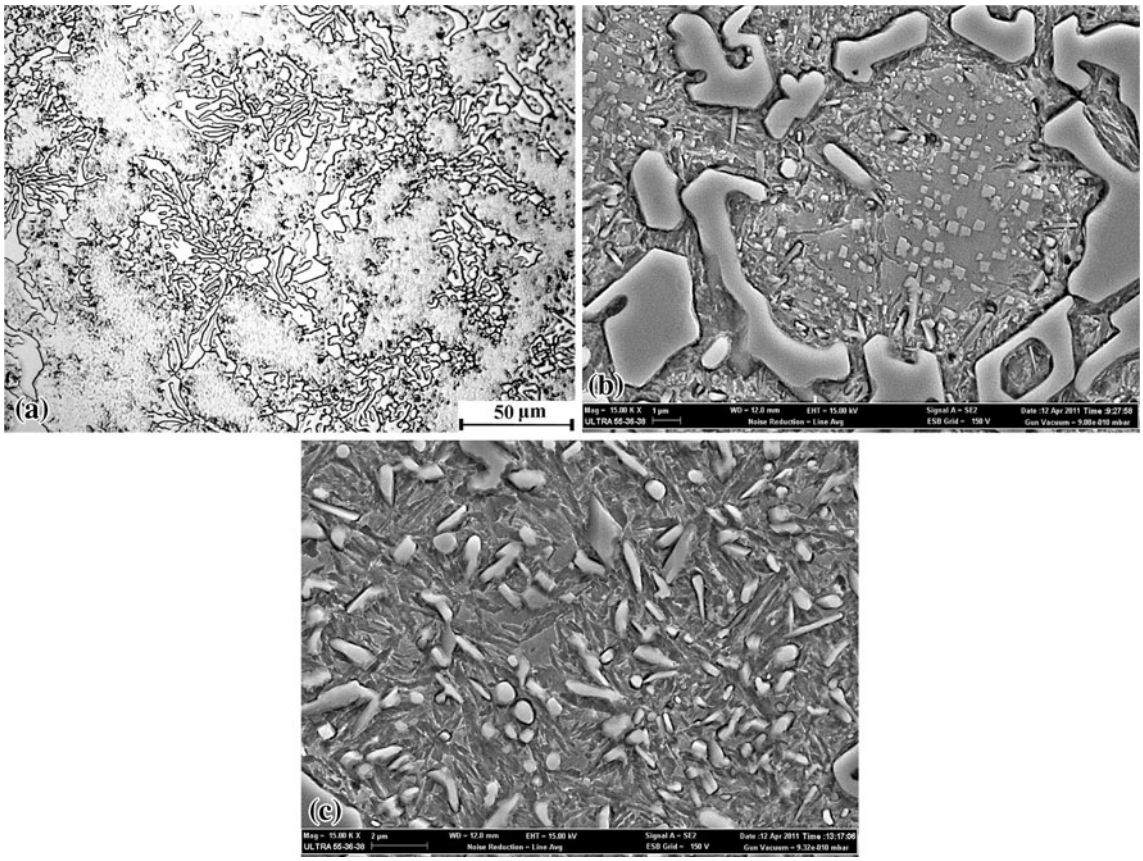

Fig. 4 Microstructure of cast alloy after destabilization at 950 °C for 20 min (a, b) and 6 h (c)

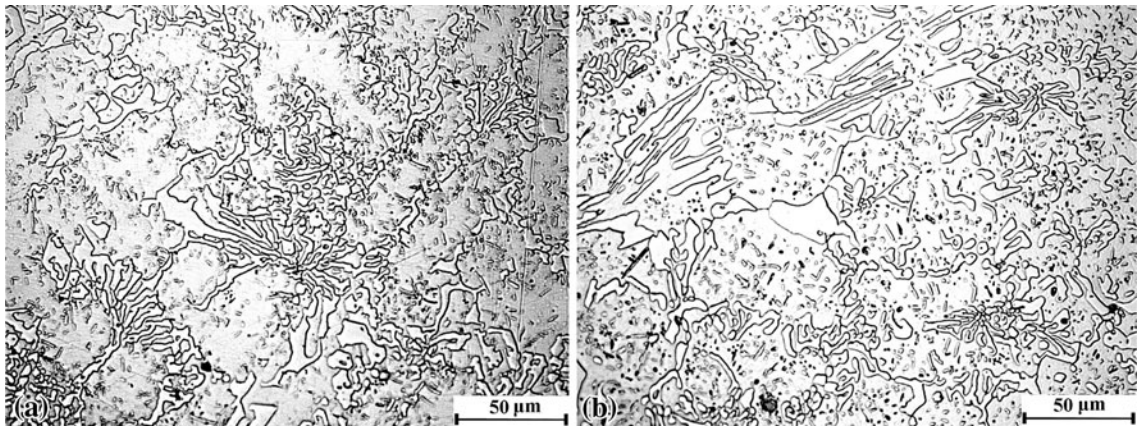

Fig. 5 Microstructure of cast alloy after destabilization at 1050 °C for 5 min (a) and 6 h (b)

temperature values of destabilized samples were found using cooling curves, obtained after soaking (Fig. 7).

Figure 8 shows that after short destabilization soaking (within incubation period), Ms was evaluated as 112-140 °C. Upon further soaking, the Ms temperature was found to be monotonically increasing up to 240-270 °C. From Fig. 8, it can be seen that individual experimental points related to the different temperature soaking times make a general scatter band of correlation ''destabilization temperature—Ms'', but some points (relating to long soaking at 950-1050 °C) lie above the averaging curve. It can be explained by surface decarburization, resulting in a seeming increase of Ms temperature.

3.4 Bulk Hardness of the Alloy After Destabilization

The rise in Ms temperature affects martensite transformation followed by the increase of bulk hardness of alloy. Figure 9 shows the curves of cast iron hardness as a function of destabilization time at different temperatures. As can be seen, soaking at any destabilizing temperature causes the hardness increase relative to

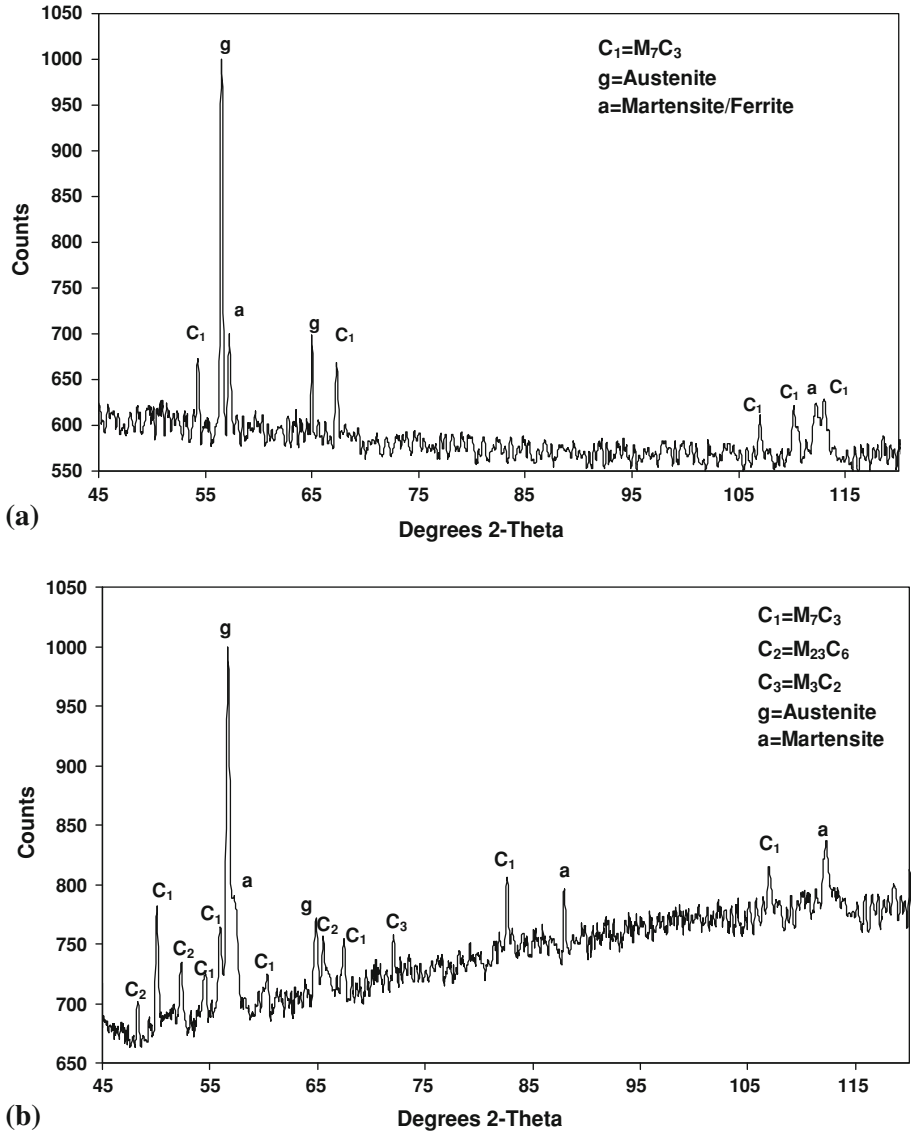

Fig. 6 XRD pattern of as-cast alloy sample (a) and after destabilization at 950 °C for 4 h (b)

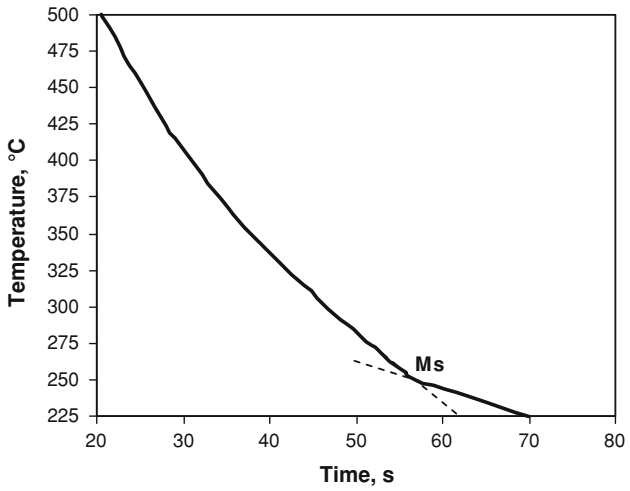

Fig. 7 Cooling curve of sample destabilized at 950 °C for 160 min

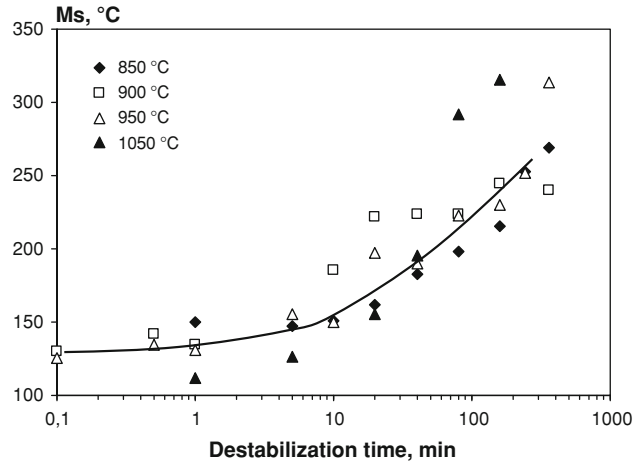

Fig. 8 Ms temperature as a function of soaking time during the destabilization heat treatment

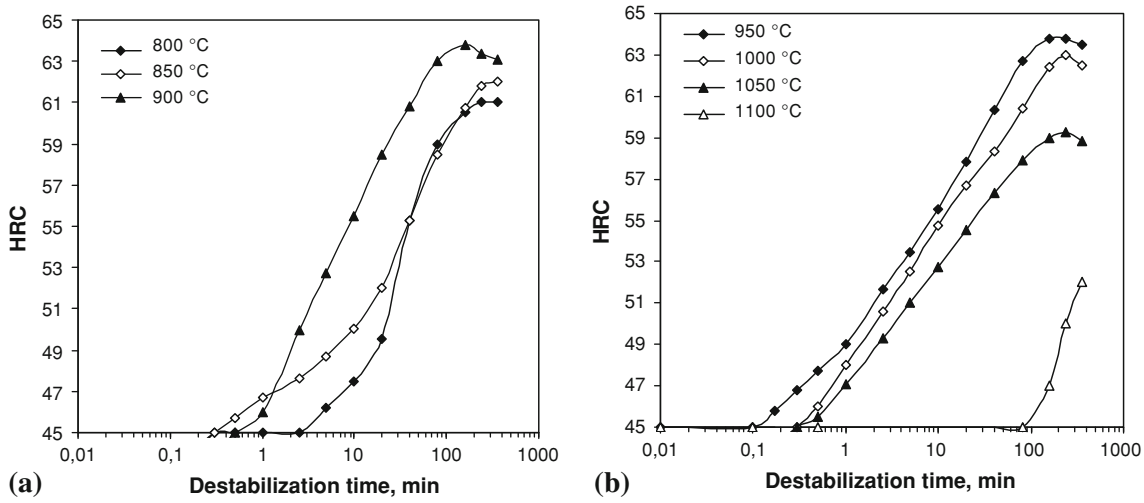

Fig. 9 Bulk hardness of the alloy as a function of the soaking time during the destabilization heat treatment

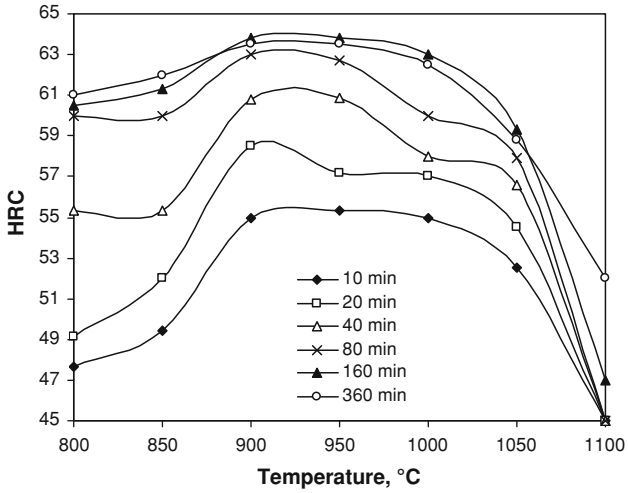

Fig. 10 Bulk hardness of the alloy as a function of destabilization temperature and soaking times

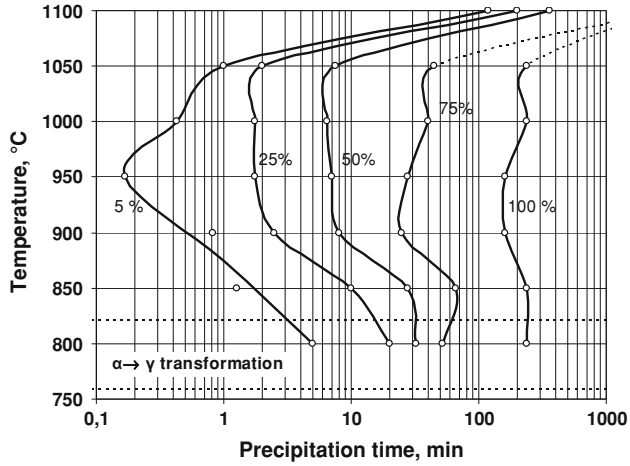

Fig. 11 TTT-diagram for precipitation process in alloy

as-cast condition (45 HRC). Herewith, every curve has an incubation period during which hardness is not changing.

At 800 °C, the hardness starts to increase after 5-min soaking; maximum hardness value (61 HRC) is reached after 6-h soaking. At 850 °C, the incubation period lasts for about 1 min, with hardness reaching up to 62 HRC after the maximum soaking. Destabilization at 900 °C results in the maximum hardness rising up to 63.5 HRC, the incubation period at this temperature is 0.5 min. Most rapidly (just after 10 s soaking) hardness began to increase at 950 °C reaching maximum 64 HRC. At higher destabilization temperatures the increasing of incubation period is observed, as well as decreasing of maximum hardness value. Thus, at 1000 and 1050 °C incubation period increased to 0.5 and 1.0 min, respectively, and the maximum hardness value was 63 HRC and 59.5 HRC, respectively. During soaking at 1100 °C the first hardness change was noted only after 2 h of destabilization, after 6 h soaking hardness reached just 52 HRC. The highest hardness value at any destabilization duration corresponds to temperature range of 900-950 °C (Fig. 10).

After rising at first stage of destabilization hardness tends to become stable (800, 850 °C) or even to reduce when soaking for 4-6 h at 900-1050 °C. According to Fig. 10 it is evident that precipitation process mostly completes after 160-min soaking (except the destabilization at 1100 °C).

Taking into account the microstructure changing described above it can be concluded that bulk hardness rising after destabilization is resulted by appearance of martensite and dispersion hardening because of carbides precipitation. At higher destabilization temperatures more austenite and less secondary carbides retain in matrix leading to bulk hardness decrease.

3.5 Kinetics of Secondary Carbides Precipitation

As the increase of hardness is obviously effected by precipitation of secondary carbides, the kinetics of this process was estimated by the obtained hardness-changing data. The hardness curves were reproduced into the kinetics curves assuming that the moment of hardness stabilization corresponds to the completion (100%) of the precipitation process at certain temperature. Following the analysis of kinetics curves the

"Time-Temperature Transformation" diagram for precipitation of secondary carbides in cast iron studied was built (Fig. 11).

As can be deduced from Fig. 11, the destabilization temperature increase of up to 950 °C intensifies the precipitation of secondary carbides in the studied cast iron. Presumably, it could be explained by activation of carbide-forming elements atoms diffusion involved into M_7C_3 carbides formation. Kinetics maximum corresponds to 950 °C where the first secondary carbides appear after 10-s soaking, and the process is completed after about 2.5-h soaking followed by coarsening of carbides particles.

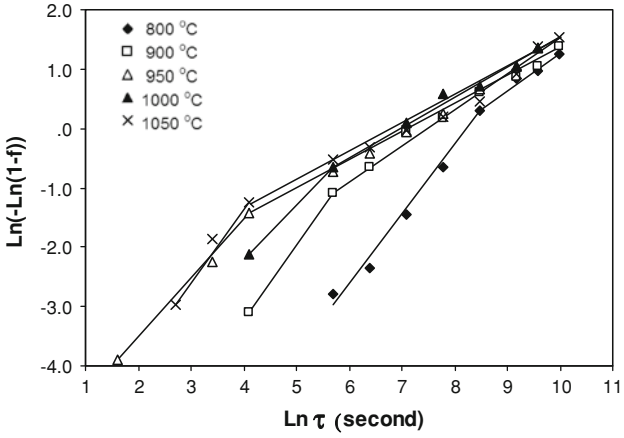

Fig. 12 The secondary carbide precipitation kinetics after taking double logarithm of fraction transformed

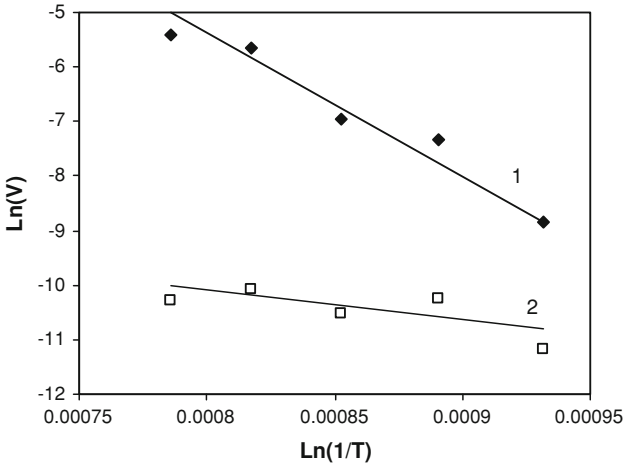

Fig. 13 Mathematical relationship for activation energy calculations: 1—carbides nucleation stage of precipitation; 2—carbides growth stage

The holding at 1000-1100 °C leads to further enhancing of atoms diffusion in austenite, but the precipitation process becomes slower, and it does not reach the completion attributed to 950 °C soaking. In this case, the influence of the other factor can be seen. That is, the growth of carbon solubility in γ-phase under destabilizing temperature increasing, the most notably seen at 1100 °C. Thus, changes of precipitation of secondary carbides kinetics at destabilization is controlled by two competing factors, namely the diffusion activity of carbide-forming elements and solubility of carbon in austenite. The superposition of these factors gives a maximum of precipitation rate at 950 °C.

The study of precipitation kinetics was carried out according to Johnson–Mehl–Avrami equation $f = 1 - \exp(-k\tau^n)$, where f is the degree of process completion for time τ. After double-taken logarithm, the kinetics curves were presented by straight lines which consist of two sections with different slopes relatively the time axis (Fig. 12).

The results show that secondary carbides precipitation proceeds in two stages. The slope of the straight lines is equal to the exponent n in Avrami's equation, which characterizes the features of process mechanism. Table 2 shows the n values for each stages of austenite decomposition. At the first stage of precipitation at all temperatures the n value is in the range 0.98-1.25, which according to Kahn's theory (Ref 15), corresponds to the nucleation of acicular and plate-like particles on the borders and edges of the grains. In the second stage the n value varies in the range 0.48-0.78, which is attributed to thickening of plates and needles. At 800 °C the nucleation stage is replaced by the stage of growth after 80 min soaking. With increasing of precipitation temperature the nucleation stage is completed faster: at 850-900 °C—after 5 min, at 950-1050 °C—after 1 min.

The activation energy (Q) for each stage of precipitation was found using Arrhenius' equation: $V = A \cdot \exp\left(-\frac{Q}{RT}\right)$ converted to the following form:

$$\frac{Q}{RT} = T \cdot (\ln(A) - \ln(V)),$$

where Q/R is the tangent of angle slope of line $\ln(V) = f\left[\frac{1}{T}\right]$ to the axis $1/T$ (Fig. 13).

The calculation of the activation energy was made for each of line sections of the Fig. 12, assuming that

$$V = \frac{(f_f - f_{in})}{(\tau_f - \tau_{in})},$$

where f_{in}, f_f—the degrees of precipitation process completion corresponding to initial (τ_{in}) time and final (τ_f) time, respectively, Table 2.

Table 2 The values of *n* in Johnson–Mehl-Avrami's equation and the activation energy (*Q*) of the precipitation of secondary carbides

		Destabilization temperature, °C					
Stage	**Parameter**	**800**	**850**	**900**	**950**	**1000**	**1050**
Carbides nucleation	*n*	1.13	1.1	1.34	0.98	1.25	1.00
	Q	196.5 kJ/g-mol					
Carbides growth	*n*	0.62	0.78	0.48	0.53	0.49	0.54
	Q	47.1 kJ/g-mol					

It was found that Q value for nucleation and growth stages is 196.5 and 47.1 kJ/g-mole, respectively.

Both stages of the precipitation process are limited by diffusion. As secondary carbides are chromium-enriched the Cr-atoms diffusion in austenite was presumably admitted as limiting factor of precipitation process. It has been previously determined (Ref 16) that the activation energy of chromium atoms volume diffusion in austenite found for vapor Cr-plating process is 184.8 kJ/g-mol. According to Ref 10, the activation energy of secondary chromium carbides nucleation in C-Ni-Cr superalloy was found to be 213.2 kJ/g-mol; the activation energy of carbides growth stage is 51.7 kJ/g-mol. Thus, Q values obtained in the current study are close to the findings in the literature.

As the atoms' diffusion along grain boundaries is known to have significantly lower (in 4-5 times) activation energy values compared with atoms' diffusion in grain volume (Ref 16), it was suggested that the first Q value obtained (196.5 kJ/g-mole) is attributed to volume diffusion mechanism and the second Q value (47.1 kJ/g-mole)—to mechanism of grain boundary diffusion. If this assumption is true, then the precipitation process in the studied cast iron is controlled at the first stage by volume diffusion of chromium atoms, and at the second stage (Ostwald ripening process), by grain boundary diffusion. The formation of critical size nucleus requires large amount of chromium atoms that could be provided by both volume and grain boundary mechanisms of diffusion. As long as the volume diffusion is more difficult process, that is, which controls the process rate in the first stage of precipitation. After nuclei were formed, their growth supposedly could be provided just by grain boundary diffusion which is known to be more easily activated. At the same time, one can assume that Ostwald ripening process of very fine carbides particles which lie inside grains could be controlled by volumetric diffusion of chromium atoms.

4. Conclusions

1. Destabilizing heat treatment at 800…1050 °C leads to decomposition of primary austenite in as-cast Cr-Mn-Ni-Mo-V cast iron affecting the secondary carbides (M_7C_3, $M_{23}C_6$, M_3C_2) precipitation. Because of depletion of austenite by carbon and alloying elements, Ms temperature rises from 110…130 °C range to that of 270…300 °C, and martensite transformation occurs. After destabilization, the bulk hardness of cast iron increases from 45 (as-cast condition) to 63-64 HRC.
2. The kinetics of secondary carbides precipitation is presented by TTT-diagram according to which, the maximum precipitation rate is attributed to soaking at 950 °C where process starts after 10 s of soaking. The precipitation is generally completed within 160-min soaking followed by coarsening of secondary carbides and decrease in the particles number. The destabilization temperature rising from 800 to 950 °C leads to the acceleration of precipitation process because of diffusion activation of Cr atoms. When temperature rises further, the precipitation slows down because of carbon solubility growth in austenite.
3. The precipitation of secondary carbides process in the alloy can be divided into two steps. The first step is carbides nucleation that is controlled by Cr atoms volume diffusion mechanism with activation energy of 196.5 kJ/g-mol. The second step is particles' growth controlled by mechanism of grain boundary diffusion with activation energy of 47.1 kJ/g-mol.

References

1. E. Zumelzu, I. Goyos, C. Cabezas, O. Optitz, and A. Parada, Wear and Corrosion Behavior of High-Chromium (14–30% Cr) Cast Iron Alloys, *JMPTEF*, 2002, **128**(1–3), p 250–255
2. R.W. Durman, Progress in Abrasion-Resistant Materials for Use in Comminuting Processes, *Int. J. Miner. Proc.*, 1988, **22**, p 381–399
3. A. Bedolla-Jacuinde, L. Arias, and B. Hernarndez, Kinetics of Secondary Carbide Precipitation in a High-Chromium White Iron, *JMEPEG*, 2003, **12**(4), p 371–382
4. J. Wang, Z. Sun, R. Zuo, C. Li, B. Shen, S. Gao, and S. Huang, Effects of Secondary Carbide Precipitation and Transformation on Abrasion Resistance of the 16Cr-1Mo-1Cu White Iron, *JMEPEG*, 2006, **15**, p 316–319
5. A.E. Karantzalis, A. Lekatou, and E. Diavati, Effect of Destabilization Heat Treatments on the Microstructure of High-Chromium Cast Iron: A Microscopy Examination Approach, *JMEPEG*, 2009, **18**(8), p 1078–1085
6. A.E. Karantzalis, A. Lekatou, and H. Mavros, Microstructural Modifications of As-Cast High Chromium White Iron by Heat Treatment, *JMEPEG*, 2009, **18**(2), p 174–181
7. A. Wiengmoon, T. Chiruangsri, and J.T.H. Pearce, Microstructural Study of Destabilized 30 wt%Cr-2.3 wt%C high Chromium Cast Iron, *ISIJ Int.*, 2004, **44**(2), p 396–403
8. G.L.F. Powell and J.V. Bee, Secondary Carbide Precipitation in an 18wt% Cr-1 wt% Mo White Iron, *J. Mater. Sci.*, 1996, **31**, p 707–711
9. F. Maratray, Choice of Appropriate Compositions for Cr-Mo White Irons, *AFS Trans.*, 1971, **79**, p 121–124
10. G. Lothongkum, S. Ratanamahasakul, and P. Wangyao, Effect of Heat Treatment Conditions on Dynamic Parameters of Secondary Carbide Precipitation in Centrifugally Cast Iron-Base Superalloy, *Acta Metal. Slovaca*, 2005, **11**, p 54–61
11. M. Kuwano, K. Ogi, A. Sawamoto, and K. Matsuda, Studies on Precipitation Process of Secondary Carbides in High-Chromium Cast Iron, *AFS Trans.*, 1990, **98**, p 725–734
12. G. Laird, II, and G.L.F. Powell, Solidification and Solid-State Transformation Mechanism in Si Alloyed High-Chromium White Cast irons, *Metall. Trans. A*, 1993, **24A**, p 981–988
13. G.L.F. Powell and G. Laird, II, Structure, Nucleation, Growth and Morphology of Secondary Carbides in High-Chromium and Cr-Ni White Irons, *J. Mater. Sci.*, 1992, **27**, p 29–35
14. G. Laird, II, Microstructures of Ni-Hard I, Ni-Hard IV and High-Cr White Cast Irons, *AFS Trans.*, 1991, **99**, p 339–357
15. E. Machlin, *An Introduction to Aspects of Thermodynamics and Kinetics Relevant to Materials Science*, 3rd ed., Elsevier Science & Technology Books, Amsterdam, 2007, p 284
16. Yu.M. Lahtin and A.G. Rahshtadt, *Heat Treatment in Machine Building*, Mashinostrojenije, Moscow, 1980, p 288 (in Russian)